Naval Research Laboratory
Washington, DC 20375-5320

NRL/MR/6680--92-7153

X-Ray Emission From Exploded-Wire Array on SATURN

P. G. BURKHALTER
J. P. APRUZESE

Dynamics of Solids Branch
Condensed Matter and Radiation Sciences Division

J. L. PORTER

Sandia National Laboratories
Alburquerque, NM 87185

G. MEHLMAN
D.A. NEWMAN

SFA, Inc.
Landover, MD 20785

December 31, 1992

REPORT DOCUMENTATION PAGE

Form Approved
OMB No. 0704-0188

1. AGENCY USE ONLY (*Leave Blank*)	2. REPORT DATE	3. REPORT TYPE AND DATES COVERED
	December 31, 1992	

4. TITLE AND SUBTITLE

X-Ray Emission from Exploded-Wire Array on SATURN

5. FUNDING NUMBERS

6. AUTHOR(S)

P. G. Burkhalter, J. P. Apruzese, J. L. Porter,* G. Mehlman,** and D. A. Newman**

7. PERFORMING ORGANIZATION NAME(S) AND ADDRESS(ES)

Naval Research Laboratory
Washington, DC 20375-5320

8. PERFORMING ORGANIZATION REPORT NUMBER

NRL/MR/6680--92-7153

9. SPONSORING/MONITORING AGENCY NAME(S) AND ADDRESS(ES)

Office of the Chief of Naval Research
800 North Quincy Street, BCT #1
Arlington, VA 22217-5000

10. SPONSORING/MONITORING AGENCY REPORT NUMBER

11. SUPPLEMENTARY NOTES

*Sandia National Laboratory, Albuquerque, NM 87185
**SFA, Inc., Landover, MD 20785

12a. DISTRIBUTION/AVAILABILITY STATEMENT

Approved for public release; distribution is unlimited.

12b. DISTRIBUTION CODE

13. ABSTRACT (*Maximum 200 words*)

X-Ray spectra were collected from sodium imploded-wire emissions employing the 10 MA Saturn pulsed-power accelerator at the Sandia National Laboratories. The spectral profiles of the Na X and XI alpha resonance lines were determined with a high-resolution KAP (002) spectrograph while a mica crystal spectrograph was used to acquire the entire sodium K-shell emission. The computer-processed time-integrated intensity data were interpreted by comparing with theoretically-predicted spectra. A static, collisional-radiative equilibrium model incorporating multifrequency radiation transport was used to compute the spectral intensities and line shapes. The comparison between observed and calculated opacity-broadened line profiles (especially Lyman alpha) indicates the presence of small emitting regions of high-density plasma which is also consistent with time-resolved, framing-camera X-ray pinhole images. Implications of these results for the Na-Ne photopumped x-ray laser are discussed.

14. SUBJECT TERMS	15. NUMBER OF PAGES
X-ray emission	38
	16. PRICE CODE

17. SECURITY CLASSIFICATION OF REPORT	18. SECURITY CLASSIFICATION OF THIS PAGE	19. SECURITY CLASSIFICATION OF ABSTRACT	20. LIMITATION OF ABSTRACT
UNCLASSIFIED	UNCLASSIFIED	UNCLASSIFIED	UNLIMITED

NSN 7540-01-280-5500

Standard Form 298 (Rev. 2-89)
Prescribed by ANSI Std 239-18
298-102

CONTENTS

X-RAY EMISSION FROM EXPLODED-WIRE ARRAY ON SATURN

INTRODUCTION

The sodium-neon resonant photopumping system, in which the $1s^2$-$1s2p$ $^1P_1$ heliumlike alpha resonant line of Na X (11.0027 Å) pumps the $1s4p$ $^1P_1$ level of heliumlike Ne IX (11.0003 Å) has long been considered an attractive scheme for achievement of a photopumped x-ray laser.[1-12] Recently, in a series of experiments performed on Saturn, the world's most powerful Z-pinch driver, definitive evidence[13, 14] of both fluorescence and population inversion in a neon gas cell irradiated by the x-rays from a sodium pinch has been obtained. Previous indications of fluorescence, though not population inversion, had been obtained at the Naval Research Laboratory using a smaller device.[9] The current work takes advantage of the sodium wire extrusion technology originally developed at Physics International Co.[10,11]. Thus, the x-ray source emission is the plasma column formed by an imploded pure sodium wire array by the Saturn generator.

The gain achievable in Ne IX is approximately inversely proportional to the width of the Na X pump line; thus, the observed spectral line profile is of particular importance. The present work uses curved-crystal spectrographs to measure the Na X 11.0027 Å spectral line intensity and profile in conjunction with photopumping experiments in the side-by-side configuration on Saturn. The profiles of the Na X pump line and nearby lines have been measured with high resolution spectrometry and analyzed with the aid of detailed plasma atomic models. The observed spectral line profiles and intensities were interpreted by comparison with collisional-radiative equilibrium (CRE) model[3,5,8,15] calculations incorporating multifrequency transport to characterize the plasma column.

In addition to a uniform or single-parameter plasma column formation, line profile calculations were also made for composite plasmas to compare with the

Manuscript approved October 22, 1992.

spectral data. The composite-plasma calculations which include both line structure and opacity broadening effects predict features consistent with the observed line profiles.

Experimental

A. Pinhole images

Both time-integrated and time-resolved x-ray pinhole images were obtained from the sodium wire implosions on Saturn. Framing-camera images were recorded with a 12-strip microchannel-plate-intensified detector at 3 ns intervals beginning at the peak of the discharge current pulse. The instrument was operated with 50 μm pinholes at ½X magnification with a resolution of approximately 150 μm. The camera viewed 60% of the 2 cm long plasma at an angle of 35° to the normal of the plasma implosion (z-axis). The images were recorded on the Kodak type 2484 film thru a 25 μm Be window. A time-integrated image and a framed image recorded at near peak of the x-ray emission were selected to densitometer and computer process for obtaining intensity profiles (contour plots) for Saturn shots 976 and 979.

Figure 1 shows the plasma x-ray emission framing-camera images recorded for a sodium wire array implosion for Saturn shot 976. Examination of the framed images indicated that the emission intensity peaks about 12 ns after the recording begins (after the fourth frame) and that the implosion column remained fully assembled for a duration of over 10 ns. A time-resolved image and contour plot generated for the fifth frame (15 ns) are shown in Fig. 2. The emission contour plot for shot 976 indicates that the most intense emission comes from regions of ~150 μm or less in diameter; but, some intense regions (i.e. 80% of peak intensity) of a few hundred micron diameters are observed. Most of the

x-ray emission as seen from the contour plots comes from a nonuniform column of about 2 mm diameter (defined as emission with more than 40% of the peak intensity). Many small spots are seen dispersed within this 2 mm column for shot 976. For emission of 20% of the peak intensity, the plasma column varies between about 2.5 to 3.0 mm diameter.The time-integrated pinhole image and contour plot seen in Fig. 3 for shot 979 shows an implosion column of about 2 mm diameter. The distinct intense emission regions were 200 μm or larger up to about 500 μm within the irregular plasma column. In both these shots and others, the x-ray emission seems to originate and is more intense on the anode side during the first 15 ns of the plasma implosion.

B. Spectroscopy

Two curved-crystal x-ray spectrographs were used to collect time-integrated spectra from sodium wire arrays imploded in the target chamber of the Saturn pulsed-power generator. A mica crystal spectrograph, curved to a 3.8-cm radius, recorded the entire sodium spectral emission in the x-ray region between 1 and 2 keV. A potassium acid phthalate (KAP) crystal spectrograph, curved to a radius of 10 cm, was used for high resolution recording of the second-order sodium spectrum over a limited spectral region of 1.1 to 1.3 keV. Both spectrographs viewed the source emission at 35° to the normal of the pinch axis (defined by the 16 sodium wire array) and recorded emission from about 60% of the 2-cm-long imploded-plasma column. Both spectrographs were positioned at about 5 m from the plasma source. For a few of the shots some spectral data was recorded with the KAP spectrograph mounted at 4.15 m from the source.

A sodium spectrum collected with the mica crystal (shot 979) is shown in Fig 4. The intensity trace is obtained from the computer-processed film densities measured with a PDS densitometer, using published DEF film calibration[16],

published data on beryllium absorption coefficients[17], calculated integral reflection coefficients for a mica crystal[18] and modeling of the source-crystal-film geometry for the curved crystal optics.[19] The 1.1 to 1.3 keV spectral region includes the Na X heliumlike-alpha (He α) ^1P component sodium-pump line at 1127 eV and the Na XI hydrogenlike-alpha (Ly α) transition at 1236 eV. The Na XI hydrogenlike 1s-2p (Lyα) and 1s-3p (Lyβ) lines are more intense than the same transitions in the Na X heliumlike series (see Fig. 4). The free-bound recombination continuum at the Na X series limit is observed on the films and in the spectral traces in the 1500 to 1700 eV region. It was difficult to accurately measure the continuum intensity slope because of the uncertainty in the mica reflectivity values near the Al K-edge (1.56 keV) that is apparent in the trace. However, best fit curves to the free-to-bound recombination continuum slopes yielded a plasma temperature of about 200 eV. The observed spectral position of the recombination continuum edge can provide a plasma density estimate. The Na XI series ionization limit was observed to be lowered by 30.3 eV, corresponding to an electron density of $7 \cdot 10^{21} cm^{-3}$, using the ion-sphere approximation[20] for free-bound electrons recombining with nuclei of sodium hydrogenlike ions. The last series member observed in the Na XI series was the 1s-7p line.

To measure the line profiles and intensities of the alpha $1s^2$-1s2p and 1s-2p transitions, the high-resolution data was processed from the curved-KAP(002) crystal spectrograph in the spectral region 1.1 to 1.25 keV. Calculated integral reflection coefficients for the curved KAP diffraction crystal[21] were used in the computer processing to yield integrated spectral intensities of the alpha lines and their satellite structure together with line profile data. Figure 5 shows Na X and Na XI spectral line profiles in detail for a sodium wire plasma.

In Fig. 5a, the heliumlike resonance $1s^2$-1s2p ^1P transition is opacity-broadened and centered at 1127 eV. The line identified as ^3P in this figure is the optically-thin heliumlike $1s^2$-1s2p ^3P intercombination line. In Fig. 5b, the Lyman alpha (Lyα) hydrogenlike 1s-2p line at 1236 eV is both broadened and split into components for this implosion shot. The heliumlike 1s-2p satellite lines are also visible in the 1210-1240 eV spectral region. Figure 6 shows the same spectra for shot 979. The line features are sharper for the He α region and therefore the lithiumlike satellite lines are more readily identified compared to the data obtained in shot 976. The ^1P line is opacity broadened and split into two components as was evident from visual inspection of all the recorded films. The Ly_α line was split into the same four components as in shot 976 but the intensities of the line components were seen to vary.

The line widths for optically-thin lines were estimated for comparison with the observed values. The estimates were based on the observed plasma source size, the diffraction-crystal-rocking curve, and plasma thermal and pressure broadening. The FWHM line width estimates were 7.6 mÅ for He α and 9.3 mÅ for Ly α, the latter having intrinsic spin-orbit splitting components.

The experimental line widths were determined from the high-resolution spectral data by computer processing to unfold the overlapping satellite lines. Figure 7 shows the computed underlying satellite intensity distribution for the He α spectral region for shot 979. The satellite spectral intensities and line profiles yielded valuable information as to linewidths without opacity broadening and as indicators of plasma temperature. However, unfolding of the underlying satellite intensities particularly in the wing structure of the resonant lines was necessary to derive accurate line widths of the alpha lines. Figure 7 shows the observed He α spectral region for shot 979 with the satellite intensities.

The lithiumlike satellites are identified as j, k and a, d and q,r in Fig. 7 (labeled according to systematic nomenclature by A. Gabriel[22]), there are also unresolved satellites m, n and s, t as wings to the intercombination line. The wavelength positions of the satellite lines have been accurately determined in laser-produced spectra [23]. However, other satellites with higher Rydberg level spectator electrons are known to occur and are underlying the plasma-broadened α line region. The satellites labeled 1 are a wing structure to the ^1P "resonance line" resulting from higher orbit spectator electrons.

The underlying satellites have been distinctly observed in spectral data collected in line-focused laser irradiation of line-configured aluminum targets [24]. The intensity curve for the satellite lines is shown in Fig. 7 beneath the observed imploded wire sodium spectrum for shot 979. The solid curve was computer generated based on the intensities found in the laser-focus experiment, published wavelengths for the Roman lettered satellite lines and fitting with Gaussian line profiles having a 10 mÅ FWHM width line. Line widths were determined by unfolding the underlying satellite structure and curve fitting Gaussians to the two-component observed line profile of the He α ^1P opacity-broadened line.

Likewise, computer processing was used to analyze the Ly α region shown in Fig. 8 for shot 976. The satellites that have been identified in previous laser-produced emission[23] are numbered in the figure. Satellite 1 is a distinct spectroscopic transition whose line width was measured in the various sodium array shots and found to be 10 m Å. The solid-curve beneath the sodium spectrum was generated using published wavelengths and an intensity distribution having a 300 eV plasma temperature and $5 \cdot 10^{21} cm^{-3}$ plasma electron density based on the theoretical work of Seely, et al. [25]. After unfolding satellite contribution

forming wing structure, the line widths of the Ly α line were determined by curve matching Gaussians to the four line components observed in the sodium implosion spectra.

The line widths measured after computer processing are listed in Table I for Ly α and the He α ^1P resonance line. The measured Na X and Na XI line widths are of the order of 20-26 m Å (~ 2 eV) in the selected data shots. The observed line widths are larger by a factor of two or three than the estimated and the observed profiles for optically-thin lines.

ANALYSIS

A. Line Ratios

The analysis of the spectral line intensities is based on the comparison with the theoretical intensity ratios calculated assuming collisional-radiative equilibrium for estimating the plasma parameters. It is both noteworthy and important to the interpretation that the predicted line ratios for the hydrogenlike -to- heliumlike α & β line ratios are similar for both the small and large plasma diameter regions near the key parameter values of 300 eV and 10^{20} cm^{-3} ion density. Examination of Fig. 9 reveals similar α-line ratio values for a temperature of 300 eV and an ion density of mid 10^{19} to 10^{20}. Likewise for the He β/He α line ratio of 0.25-0.30 the CRE line ratios (see Fig. 10) yield 300 eV and 10^{20} for both small and large diameter plasma. In addition, the Ly β/Ly α line ratio value of 0.2 is found to be consistent for 300 eV and 10^{20} for both small and large plasma diameters(see Fig. 11). Within the agreement found in Table II, the predicted line ratios are consistent with a composite plasma formed by both small and large diameter emission regions.

Also, the fractional abundance of ionization stages can be determined from the CRE calculations vs. temperature and density. The heliumlike and hydrogenlike

abundance contours are presented in Figs. 12 and 13, respectively. From the temperature and ion density (300 eV, 10^{20}), the fractional abundances are 0.2 to 0.35 for the heliumlike and 0.50 to 0.55 for hydrogenlike ions.

B. Calculated Line Widths

The line widths were calculated for the alpha lines both assuming an optically-thin plasma and for a wide range of plasma sizes but only for plasma conditions consistent with the line intensity analysis. Table III lists the line widths for the several plasma conditions. The first line is for optically-thin conditions and yields a value of 10 mÅ for Ly alpha in agreement with the hand-calculated estimate and the value of 4 mÅ for He alpha that is about one-half the estimate. The line widths were also calculated at the same plasma conditions for a 110 μm (small diameter) and for a 1-mm large diameter plasma. Furthermore, the line widths were calculated for two composite plasmas of both small and large size plasma emission regions. The calculated line profiles for the two alpha lines are shown in Figs. 14 and 15.

DISCUSSION AND COMPARISON

In the present work, the observed x-ray emission from sodium wire arrays shows spectral profile characteristics consistent with small intense emitting regions of 150 μm diameter or less within a large-diameter, nonuniform plasma column. The temperatures derived from CRE calculations and satellite-to-resonance line ratios were 250-310 eV while the temperature from the recombination slope was about 200 eV. The fact that the intense emitting regions correspond to a high plasma density is observed and verified from the ionization lowering of the series limits of the hydrogenlike and heliumlike ionization stages.

The pinhole images of the sodium plasma show small regions of x-ray emission within a broad plasma column defined by the intensity contours from the pinhole images. Both the framing- and time-integrated images show plasma regions of 150 μm or less.

The resonance line profiles show opacity-broadened line structure with intensities that varied shot-to-shot while maintaining the same general line-structure character. All the alpha lines were opacity broadened well beyond the instrumental and thermal linewidth broadening estimates of about 10 mÅ. The alpha line profiles were found to be 23-25 mÅ (~2 eV) at FWHM. The individual line components are narrower (about 8-10 mÅ, that is, the estimated instrumental broadening). The question was considered whether the profiles could possibly arise from physically-separated plasma sources. The He alpha line in shot 979 had resolved structure with separations of 8 mÅ between the red and blue wings centered at 11.003 Å. A plasma source separation of 4 mm would be necessary to correspond to the 9.9 mÅ line separation seen in the component splitting of the He $1s^2$ - $1s2p^1P$ line profile. This is inconsistent with the observed x-ray emission in the pinhole images. The plasma implosion column was observed as an irregular column roughly 2 mm in diameter with weak emission up to 4 mm without any evidence of emission detectable from single wires in the peripheral regions.

The linewidths of individual satellite lines and the approximate linewidths of the individual components in the resonance lines were found to be near the instrumental broadening value.

Strong evidence for minute plasma forming regions is the line structure found in the hydrogenlike Lyman alpha line seen in the various shots. The line profile structure seen in shot 976 is considerably different than the simple line structure predicted for the optically-thin case and the observed third component

or center line is predicted only in simulations for plasma diameters greater than about 1-mm. This third central component represents spectral emission between the J = 1/2 and 3/2 components from less-opaque regions. At large diameters, radiation transport thru opaque plasma is sufficient to suppress this third feature.

Similarly, densitometer-contours of x-ray pinhole images collected a decade ago[26] from an exploded aluminum-wire-array plasma generated on PITHON showed intense regions of x-ray emission with sizes varying from about 500 μm to 100 μm (pinhole limited) core regions within a nonuniform plasma column.

In photopumped x-ray lasers, the achievable gain for a given pump line power is approximately inversely proportional to the pump line width, assuming that the pumping and pumped lines remain overlapped in the absence of energy-shifting of the coincident levels. Previous gain calculations[8, 9, 12-14] for the Na-Ne scheme have assumed widths of 0.8-1.3 eV at peak pump power. The present time-integrated measurements give a full-width at half maximum of 2.0-2.9 eV. If the width at peak pump power is the same as the time-integrated width, the calculated gain is indeed reduced by factors of 2-3. However, the width at peak power may well be closer to the previous 0.8-1.3 eV estimates than the present 2.0-2.9 eV time-integrated measurements. Previous time resolved measurements of sodium and aluminum pinches[11,27] using the Double-EAGLE device of Physics International Corp. have revealed peak Lyα/Heα ratios of ~4 rather than the 2 obtained by time-integrated spectroscopy in the present experiments. It is certain that the peak Saturn Lyα/Heα ratio is somewhat greater than the time integrated value of 2, and a reasonable assumption can be made that this peak ratio is also 4. Using the CRE model to fit the higher ratio reduces the calculated He-like fraction to as low as 3%. Peak power, however, is not reduced because the increase in

temperature from ~300 to 600 eV increases the collisional excitation coefficient of the 1s2p level, and also reduces the line opacity. The calculated He α profile has a width of 1.0 eV, consistent with the previous assumptions, due to greatly reduced opacity broadening. Only time-resolved high resolution spectroscopy can reveal the actual pump line width at peak power, but as discussed above, there are sound experimental and theoretical reasons to expect that it is smaller than the time-integrated width.

CONCLUSIONS

The alpha line shapes from the sodium wire arrays have broadened line profiles characteristic of plasma opacity effects. The structure of the Lyman alpha lines is in reasonable agreement with modeling of small diameter (100 μm) emission regions. The opacity-broadened line widths correspond to predictions for large-diameter (few mm) plasmas. The helium-and hydrogen-like alpha line profiles agree with the CRE multifrequency-transport model simulating a composite plasma having a high-ion density ($6 \cdot 10^{20}$ cm^{-3}) for the small diameter (~ 100 μm) plasma spots and a lower ion density ($5 \cdot 10^{19}$ to $1 \cdot 10^{20}$ cm^{-3}) for a large diameter (~ 2-mm) plasma-column; both regions have a plasma temperature of about 300 eV derived from to the Lyα/Heα line ratios.

The framing pinhole camera data give supporting evidence for a composite-density plasma formation utilized for modeling the sodium wire array plasmas. The pinhole images, collected near peak-intensity plasma emission, show small, intense-plasma-emission regions embedded in a 2-mm diameter, non-uniform, plasma-column.

ACKNOWLEDGMENTS

We wish to thank Sam Lopez and Mark Vargas for their assistance in the mounting and the alignment of our spectrographs and John McGurn for helping acquire the pinhole-camera data. The authors wish to acknowledge the entire Saturn crew for their efficient operation of the Saturn accelerator. We also are grateful to Larry Ruggles and Rick Spielman at Sandia for valuable discussions regarding this work.

This work was performed in part under the auspices of the Strategic Defense Initiative Organization.

REFERENCES

a) Present address: Lawrence Livermore National Laboratory, P.O. Box 808, Livermore, CA 94550

(1) A. V. Vinogradov, I. I. Sobelman, and E. A Yukov, Kvant. Elektron (Moscow) 2, 105 (1975) [Sov. J. Quantum Electron. 5, 59 (1975)].

(2) P. L. Hagelstein, University of California Report No. UCRL-53100, 1981 (unpublished).

(3) J. P. Apruzese, J. Davis, and K. G. Whitney, J. Appl. Phys. 53, 4020 (1982).

(4) P. L. Hagelstein, Plasma Phys. 25, 1345 (1983).

(5) J. P. Apruzese and J. Davis, Phys. Rev. A 31, 2976 (1985).

(6) R. C. Elton, T. N. Lee, and W. A. Molander, Phys. Rev. A33, 2817 (1986).

(7) F. C. Young et al., Appl. Phys. Lett. 50, 1053 (1987).

(8) J. P. Apruzese et al., Phys. Rev. A 35, 4896 (1987).

(9) S. J. Stephanakis, J. A. Apruzese, P. G. Burkhalter, G. Cooperstein, J. Davis, D. D. Hinshelwood, G. Mehlman, D. Mosher, P. F. Ottinger, V. E. Scherrer, J. W. Thornhill, B. L. Welch, F. C. Young, IEEE Transactions on Plasma Science 16, 472 (1988).

(10) C. Deeney, R. R. Prasad, T. Nash, and N. Knobel, Rev. Sci. Instrum. 61, 1551 (1990).

(11) C. Deeney, T. Nash, R. R. Prasad, L. Warren, and J. P. Apruzese, Appl.

Phys. Lett. 58, 1021 (1991).

(12) J. Nilsen and E. Chandler, Phys. Rev. A 44, 4591 (1991).

(13) J. L. Porter, R.B. Spielman, M.K. Matzen, E.J. McGuire, L.E. Ruggles, M.F. Vargas, J.P. Apruzese, R.W. Clark and J. Davis, Phys. Rev. Lett. 68, 796 (1992).

(14) J. P. Apruzese et al, in X-Ray Lasers 1990, Institute of Physics Conf. Series No. 116, edited by G. J. Tallants (IOP, Bristol, England, 1991), p. 39.

(15) J. P. Apruzese, P. C. Kepple, K. G. Whitney, J. Davis, and D. Duston, Phys. Rev. A24, 1001 (1981).

(16) P. D. Rockett, C. R. Bird, C. J. Hailey, D. Sullivan, D. B. Brown, and P. G. Burkhalter, Appl. Optics 24, 2536 (1985).

(17) B. L. Henke, P. Lee, T. J. Tanaka, R. L. Shimabukuro, and B. K. Fujikawa, Atomic Data and Nuclear Data Tables, Vol. 27, No. 1, 1 (1982).

(18) B.L. Henke, Rev. Sci. Instrum. 56 (8), 1551 (1985).

(19) J. W. Criss, Appl. Spectrosc. 33, 19 (1979).

(20) J. C. Steward and K. D. Pyatt, Astrophys. J. 144, 1203 (1966).

(21) D. B. Brown and M. Fatemi, J. Appl. Phys. 51, 2540 (1980).

(22) A. H. Gabriel M.N.R.A.S., 160, 99 (1972).

(23) U. Feldman, G.A. Doschek, D.J. Nagel, R.D. Cowan, and R.R. Whitlock, Astrophys. J 192, 213 (1974).

(24) P. G. Burkhalter, J. P. Apruzese, and D. Duston, in "Radiative Properties of Hot Dense Matter III", edited by B. Rozsnyai, C. Hooper, R. Cauble, R. Lee, and J. Davis (World Scientific, Singapore, 1987).

(25) J.F. Seely, At. Data and Nuclear Tables 26, 137 (1981).

(26) P. Burkhalter, J. Davis, J. Rauch, W. Clark, G. Dahlbacka, and R. Schneider, J. Appl. Phys. 50, 705 (1979).

(27) F. C. Young, D. D. Hinshelwood, J. P. Apruzese, C. Deeney, T. Nash, and R. R. Prasad, J. Appl. Phys. 69, 7520 (1991) and C. Deeney, private communication (1991).

Table I. Experimental Line Widths

Shot	Lyα* (mÅ)	(eV)	Heα* (mÅ)	(eV)
974	19.5	2.4	19.5	2.0
975	23.6	2.9	22.3	2.3
976	21.7	2.7	24.7	2.5
977	26.3	3.2	23.8	2.4
978	21.1	2.6	26.0	2.6
979	20.3	2.5	22.0	2.2

Note: Satellite labeled 1 for the Lyα line (see Fig. 8) has a line width of 10 mÅ.

*F.W.H.M. of Gaussian fitting.

Table II. Line Ratio Matching Comparison of Observed and Predicted.

Line Ratio	Experimental (Shot 979)	Theoretical*
Lyα/Heα	2.3	2.3
$^3P/^1P$	0.083	0.073
Lyβ/Lyα	0.15	0.26
Heβ/Heα	0.19	0.31

*Theoretical (CRE) line intensity ratio calculations for a composite plasma at a temperature of 300 eV; bright regions (100-μm diameter "spots") at $6 \cdot 10^{20}$ ions/cm^3; uniform plasma column (2-mm diameter) at $5 \cdot 10^{19}$ ions/cm^{-3}.

Table III. Calculated Line Widths for Single-and Composite-Plasma Conditions

Plasma Conditions			Lyα		Heα	
Te	N_I	Diam.	(mÅ)	(eV)	(mÅ)	(eV)
310 eV	$3 \cdot 10^{20}$	thin	~ 7	0.8	~3	0.33
"	"	110 μm	14	1.7	10	1.0
"	"	1 mm	17.5	2.15	20	2.0
"	"	3 mm	28	3.4	32	3.3
Composite Plasma						
300 eV	$1 \cdot 10^{20}$	2 mm				
			16	2.0	15	1.5
"	$6 \cdot 10^{20}$	100 μm				
300 eV	$5 \cdot 10^{19}$	2 mm				
			15	1.8	15	1.45
"	$6 \cdot 10^{20}$	100 μm				

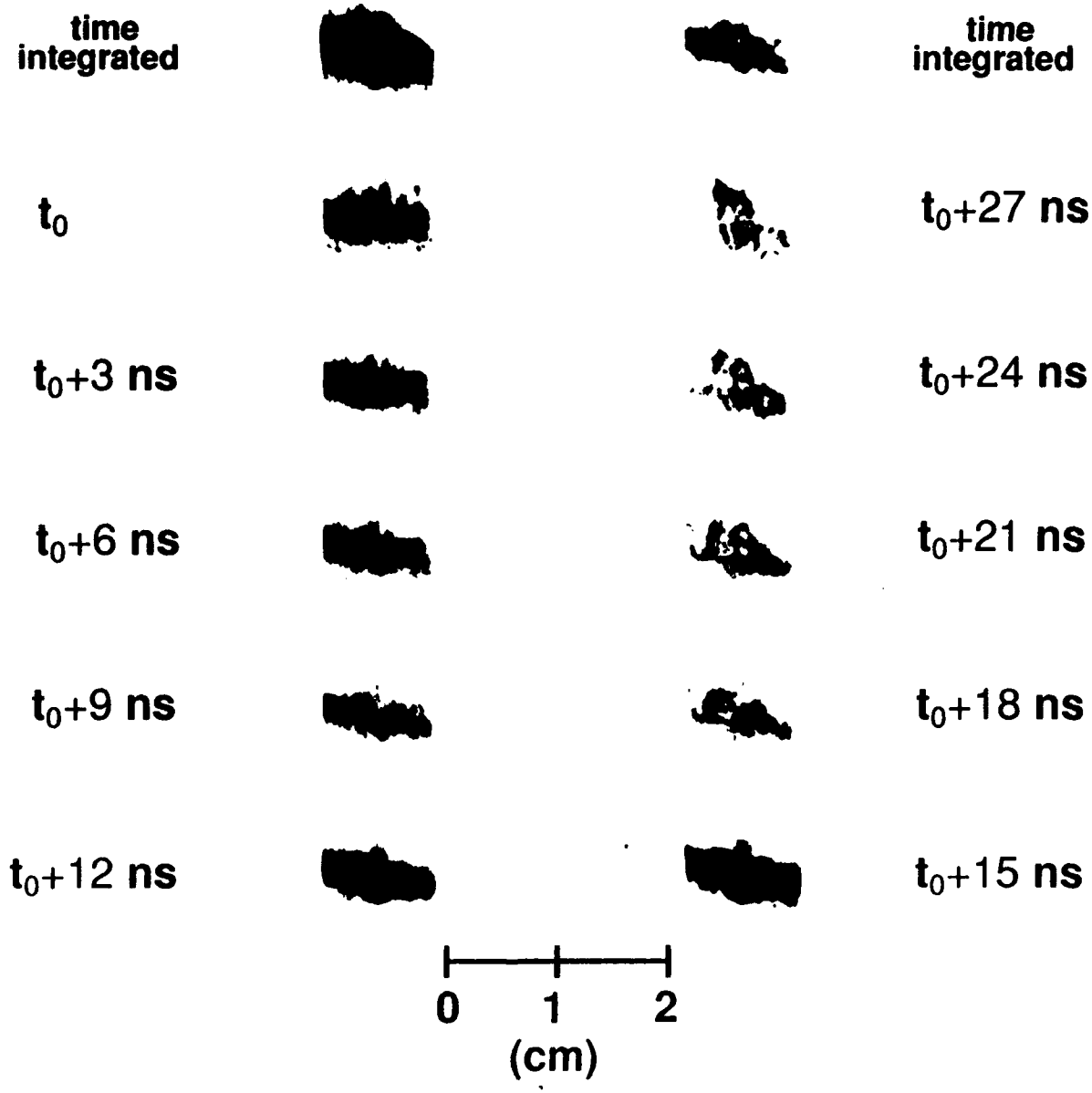

Fig. 1. Framing-camera, pinhole images of sodium wire array implosion on Saturn shot 976.

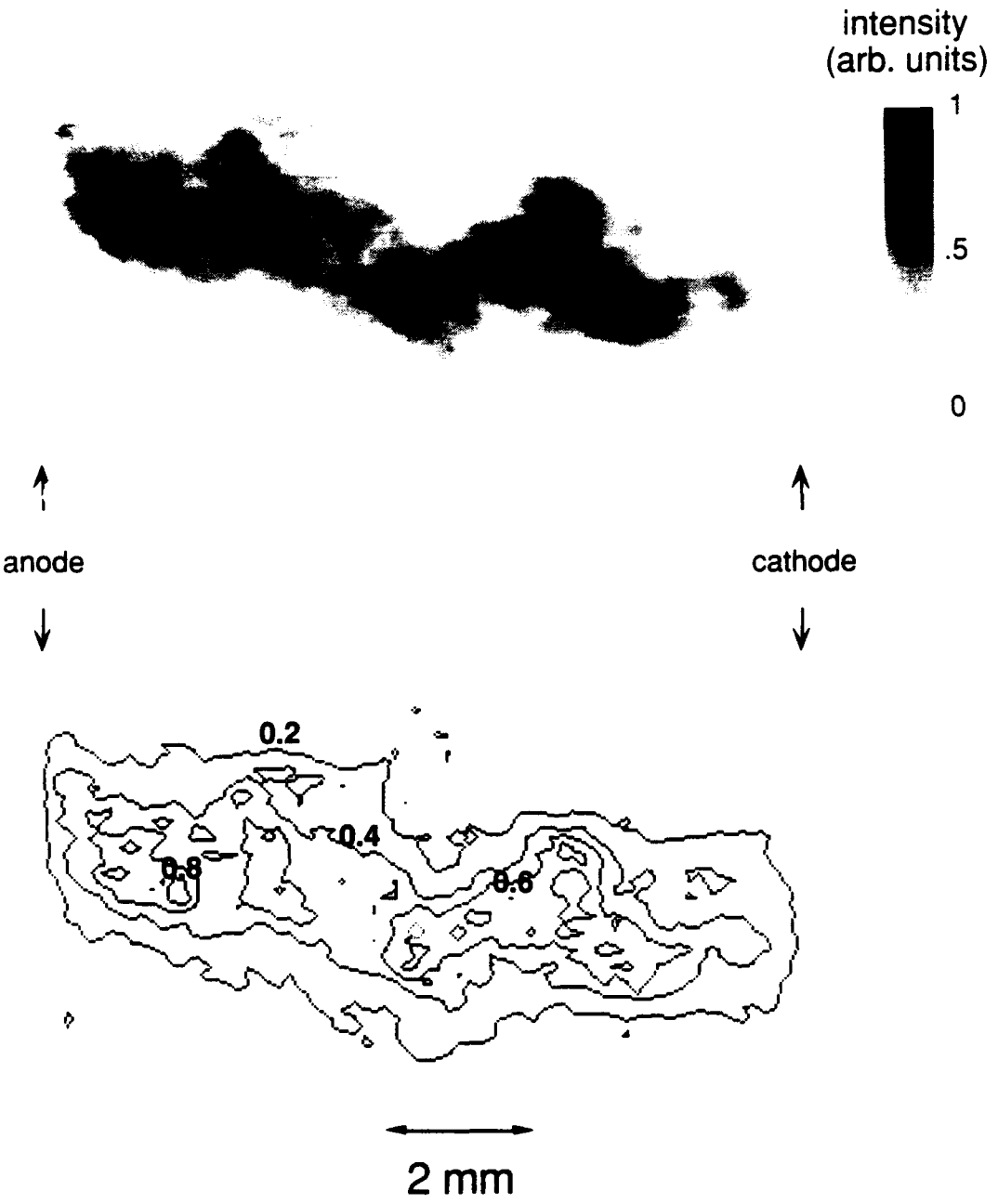

Fig. 2. Time-resolved x-ray pinhole image and densitometer contour near peak of x-ray emission on Saturn shot 976.

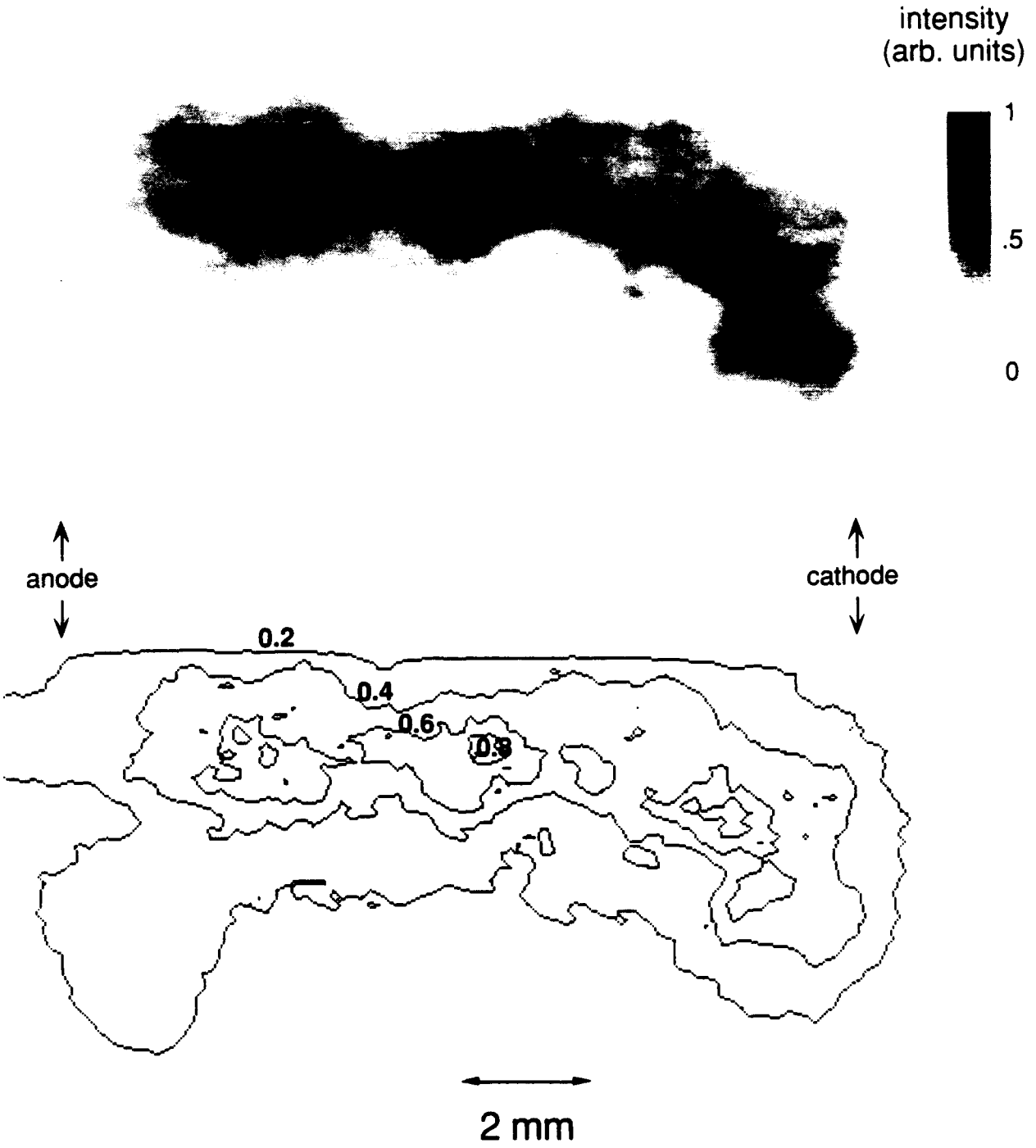

Fig. 3. Time-integrated x-ray pinhole image and densitometer contour for Saturn shot 979.

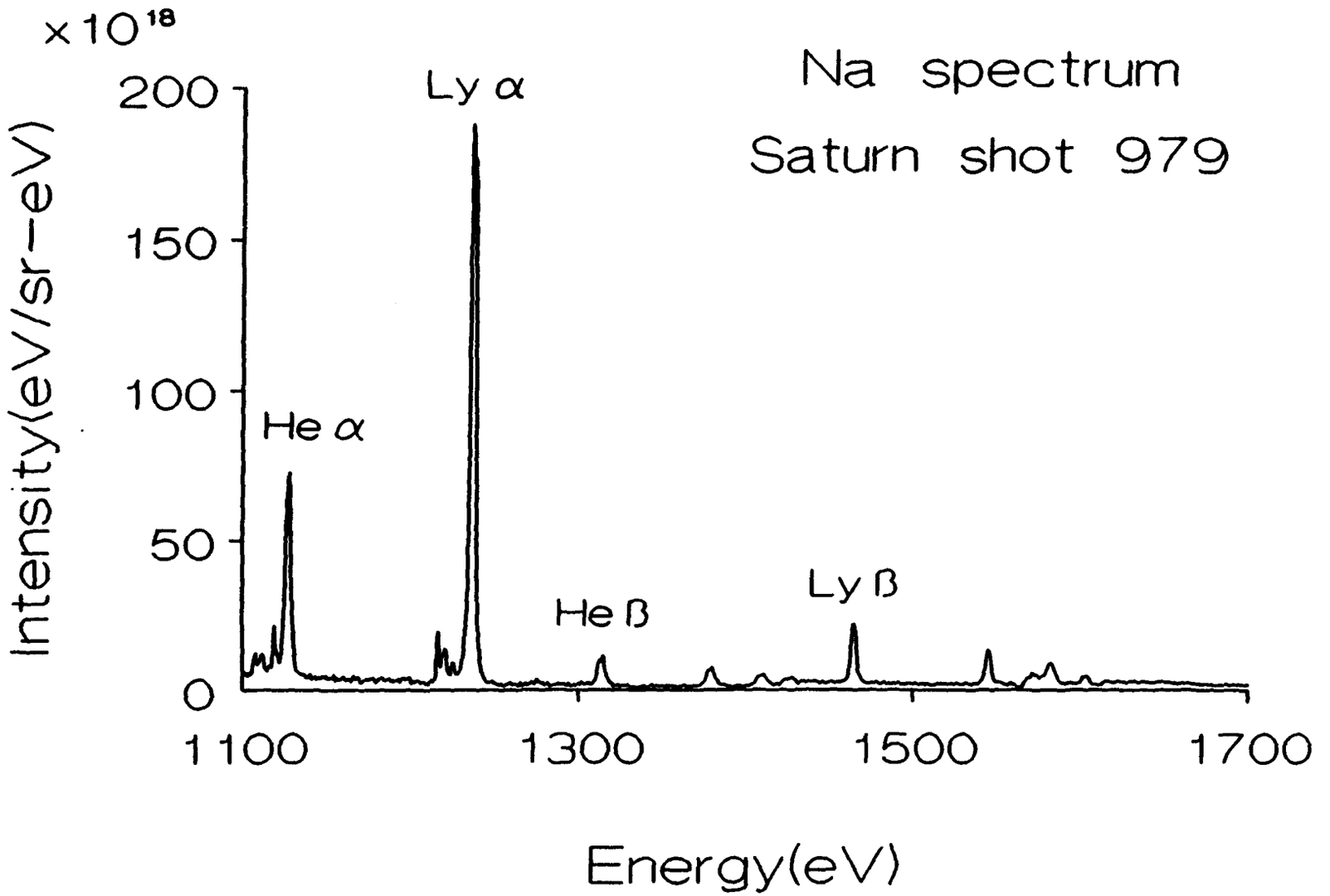

Fig. 4. Spectral emission from a sodium wire array implosion (curved-mica crystal spectrograph), for shot 979.

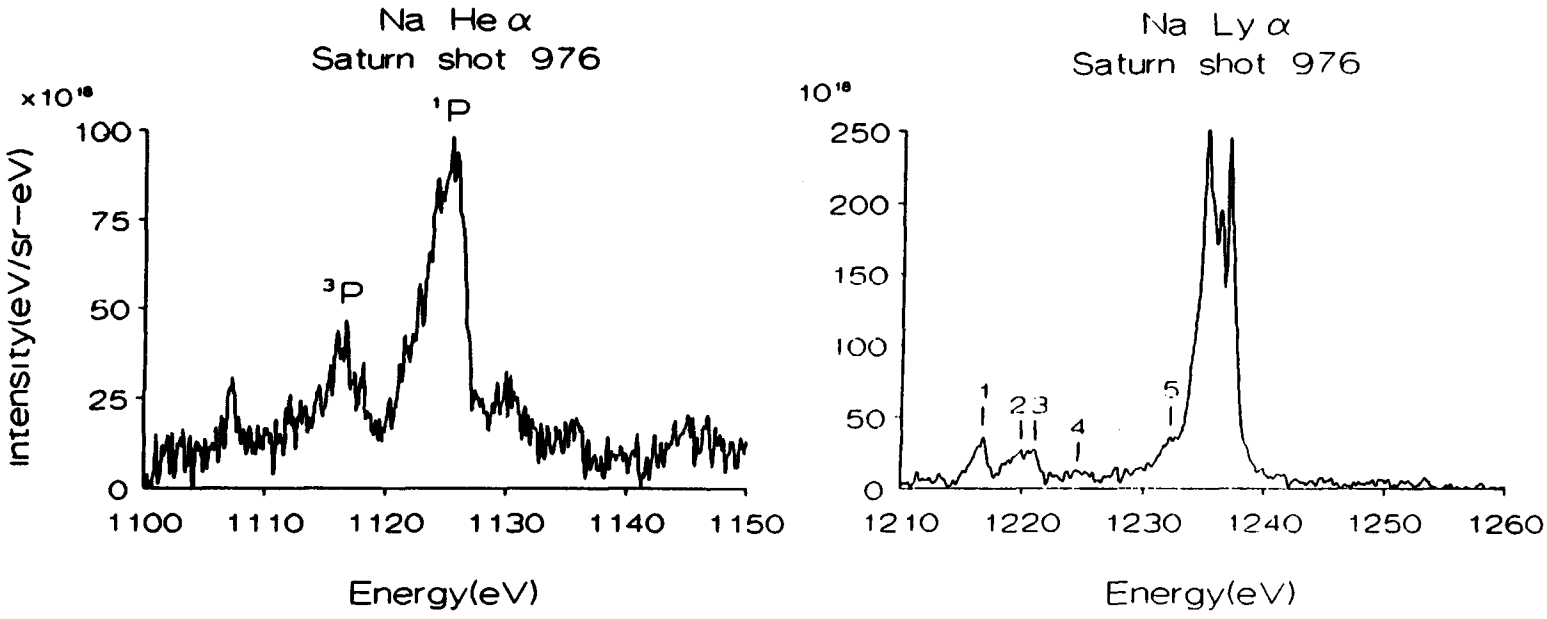

Fig. 5. **High-resolution spectral line profiles of a) the heliumlike alpha ^1P (11.003 Å) sodium pump line and b) the sodium hydrogenlike Lyman alpha (~ 10 Å) for Saturn shot 976.**

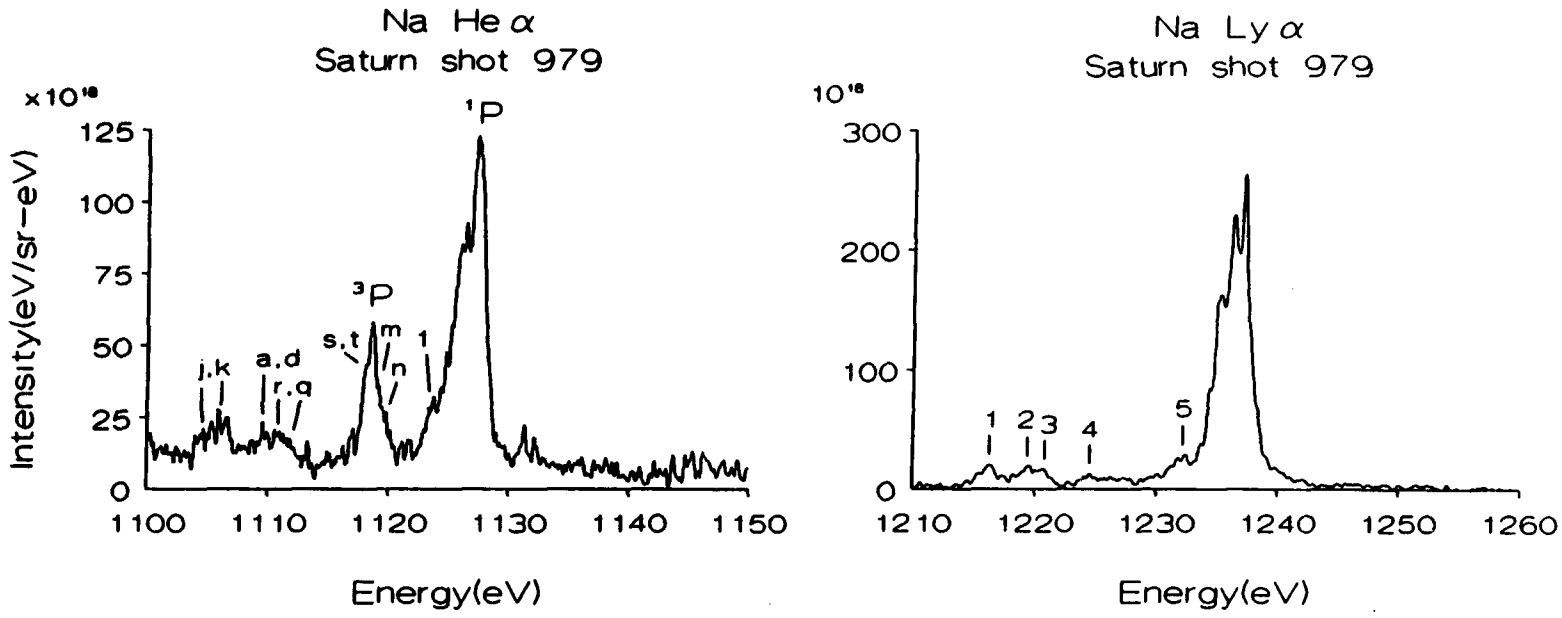

Fig. 6. High-resolution spectral profiles for the alpha lines for Saturn shot 979.

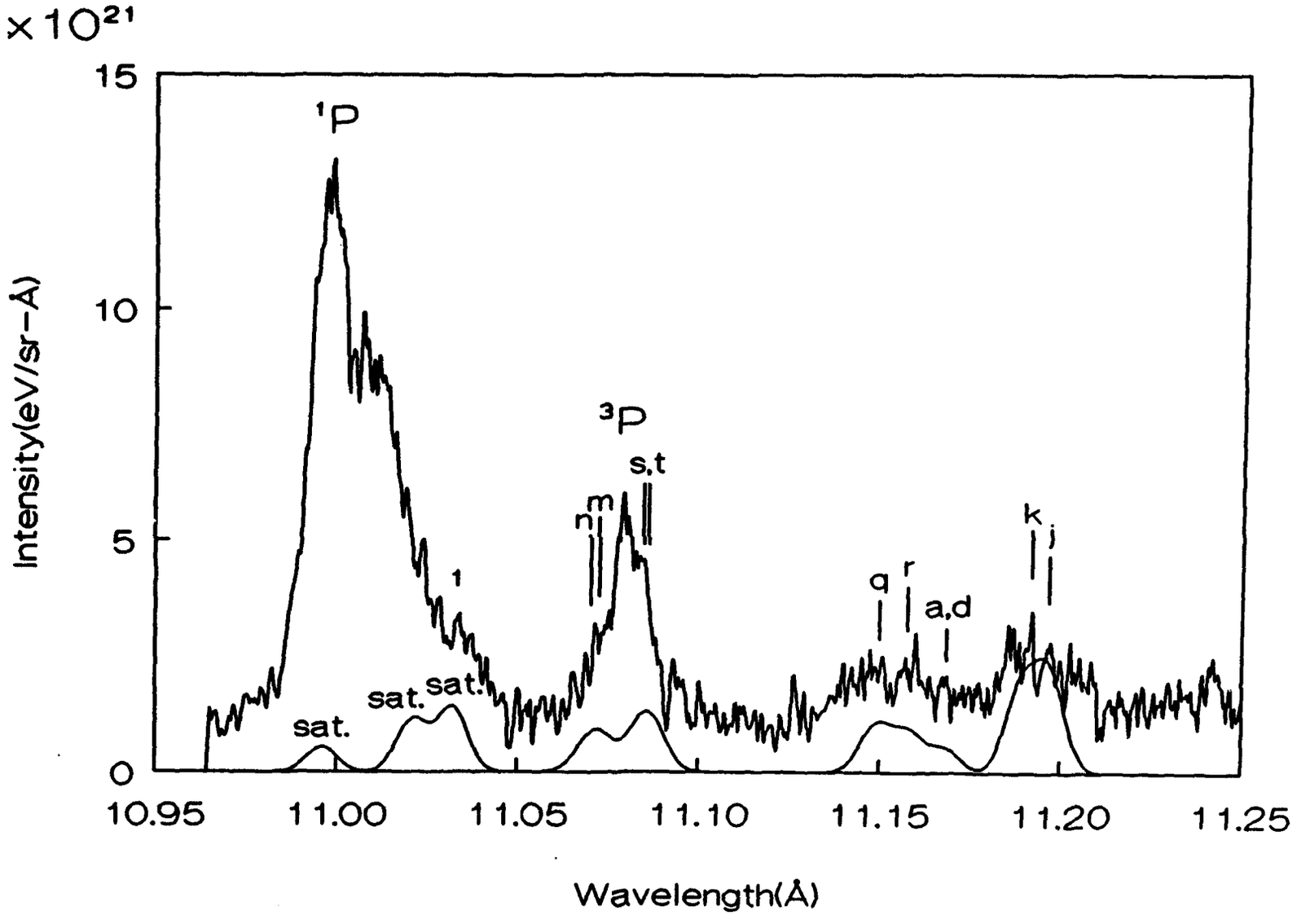

Fig. 7. Experimental Sodium Heα ^1P and ^3P lines and lithiumlike satellite intensities (labeled sat. and small Roman letters) for shot 979. The solid curve beneath the observed spectrum is computer-generated satellite spectral intensities based on observed satellite line spectral data collected from line-focused laser-matter-interaction studies.

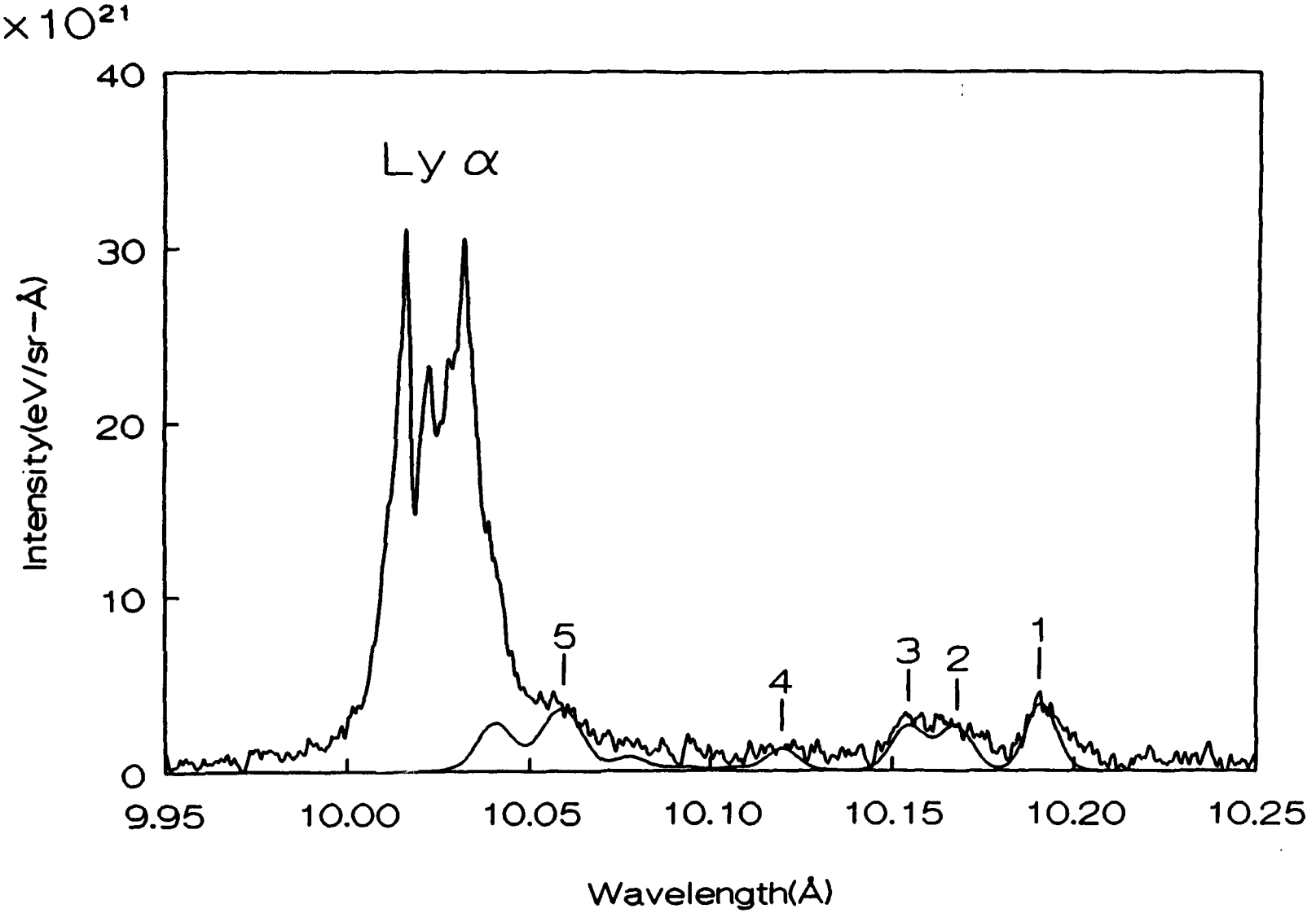

Fig. 8. Experimental sodium Lyα line and heliumlike satellite intensities for shot 976. The solid curve is the theoretically-predicted satellite spectral intensities for a plasma temperature of 300 eV.

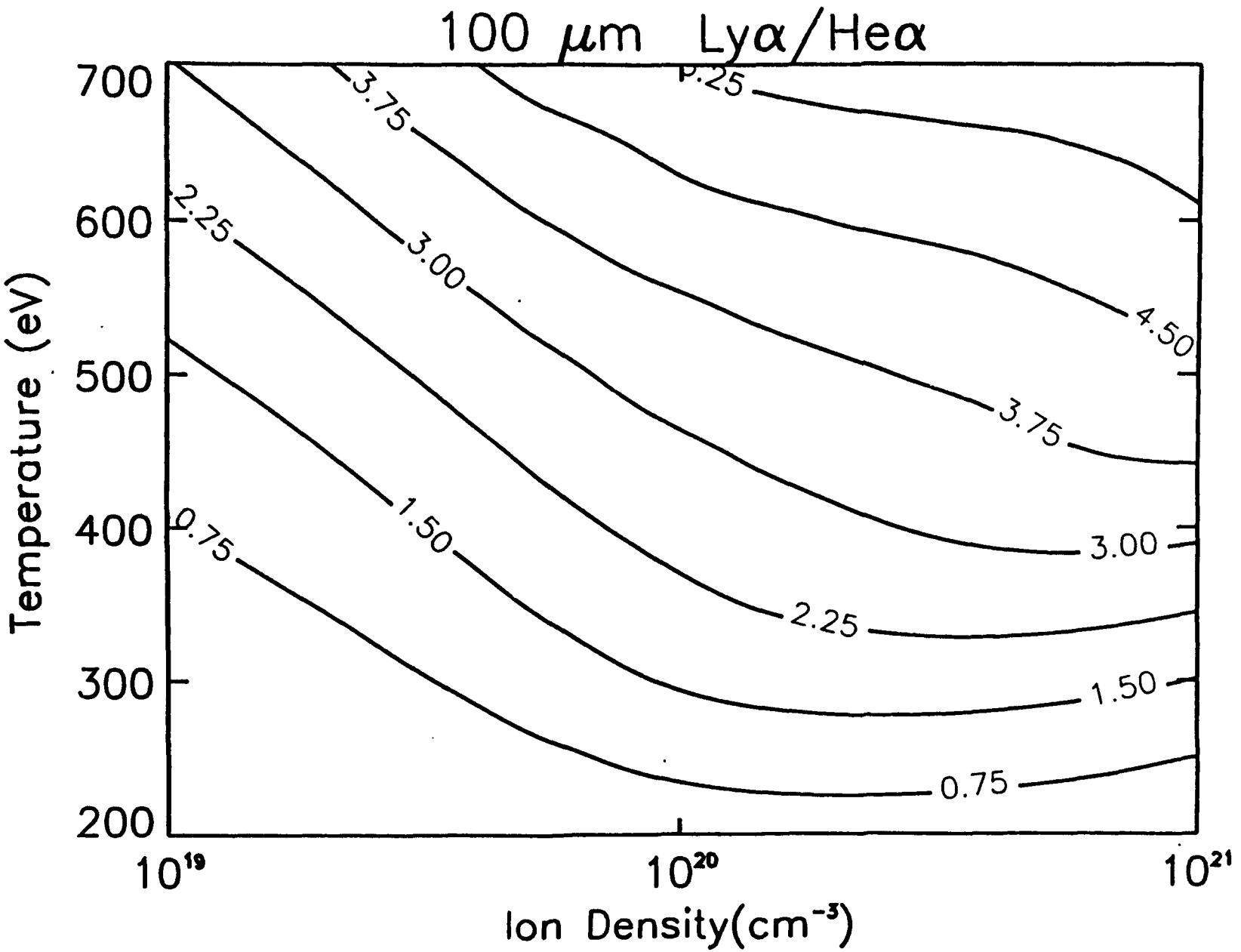

(a)

Fig. 9. Theoretical (CRE) calculated alpha line intensity ratios as a function of plasma temperature and ion density for small and large diameter plasma emission.

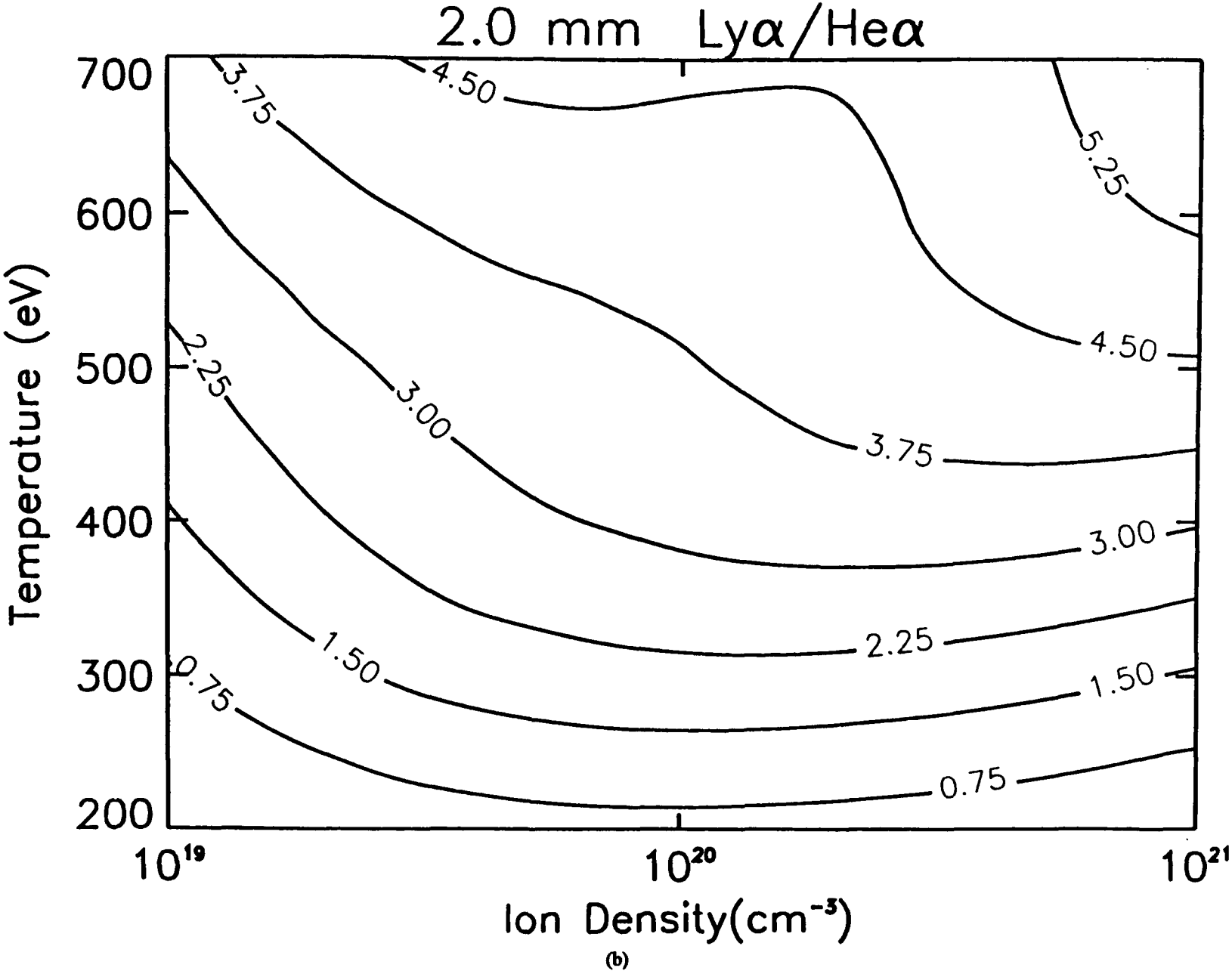

(b)

Fig. 9. (Continued) Theoretical (CRE) calculated alpha line intensity ratios as a function of plasma temperature and ion density for small and large diameter plasma emission.

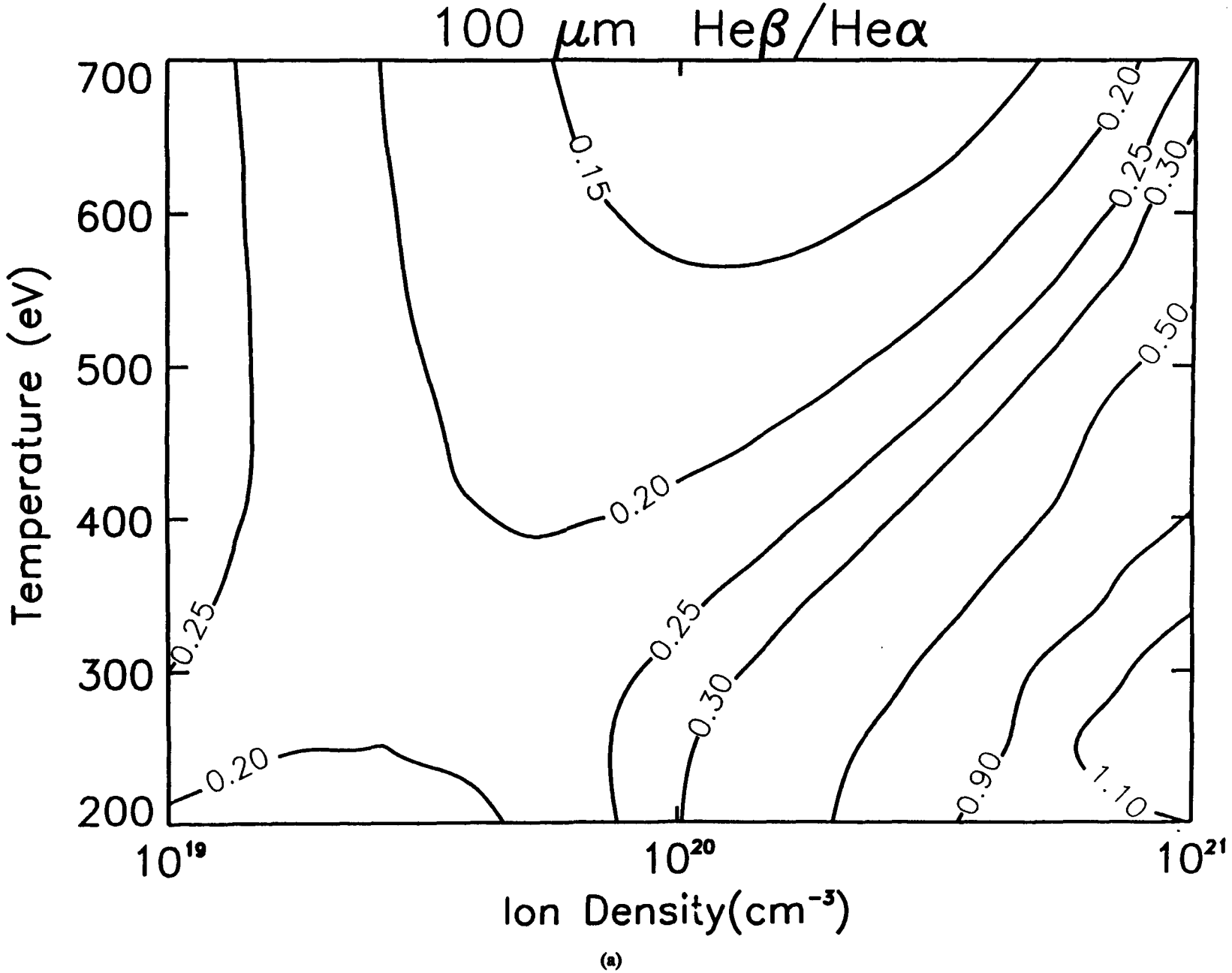

(a)

Fig. 10. Theoretical (CRE) predicted heliumlike beta/alpha line ratios.

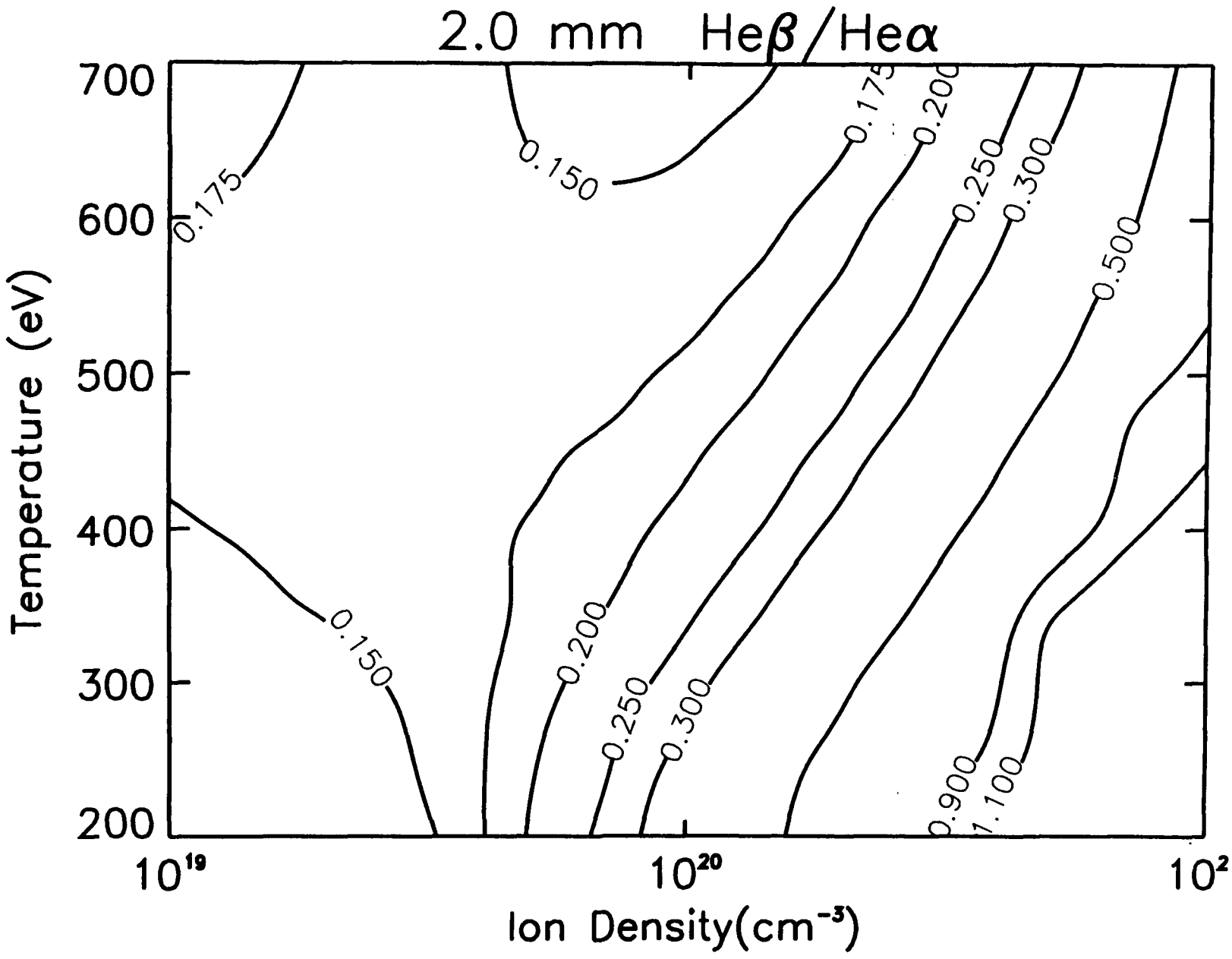

(b)

Fig. 10. (Continued) Theoretical (CRE) predicted heliumlike beta/alpha line ratios.

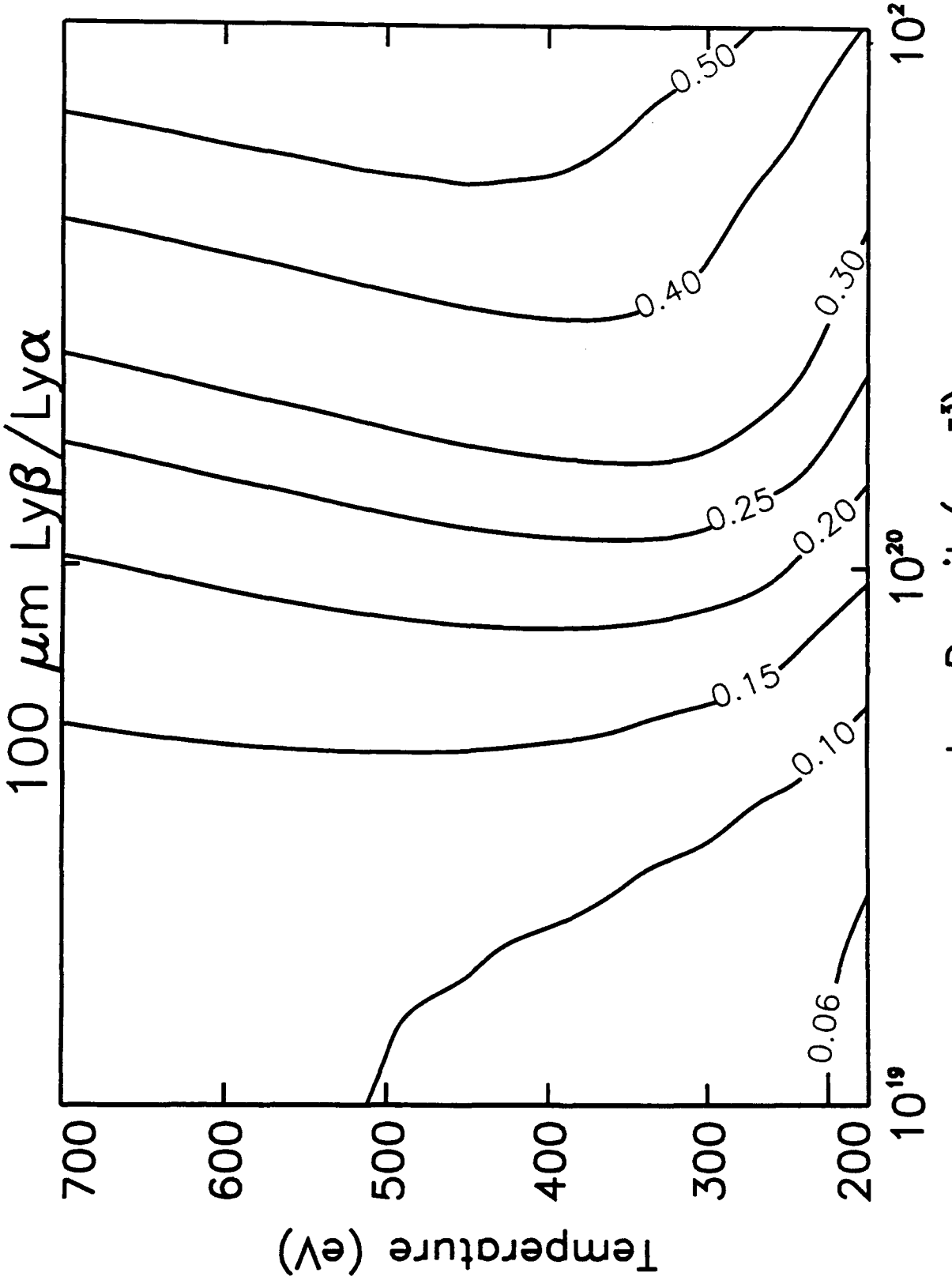

(a)

Fig. 11. Theoretical (CRE) predicted hydrogenlike beta/alpha line ratios.

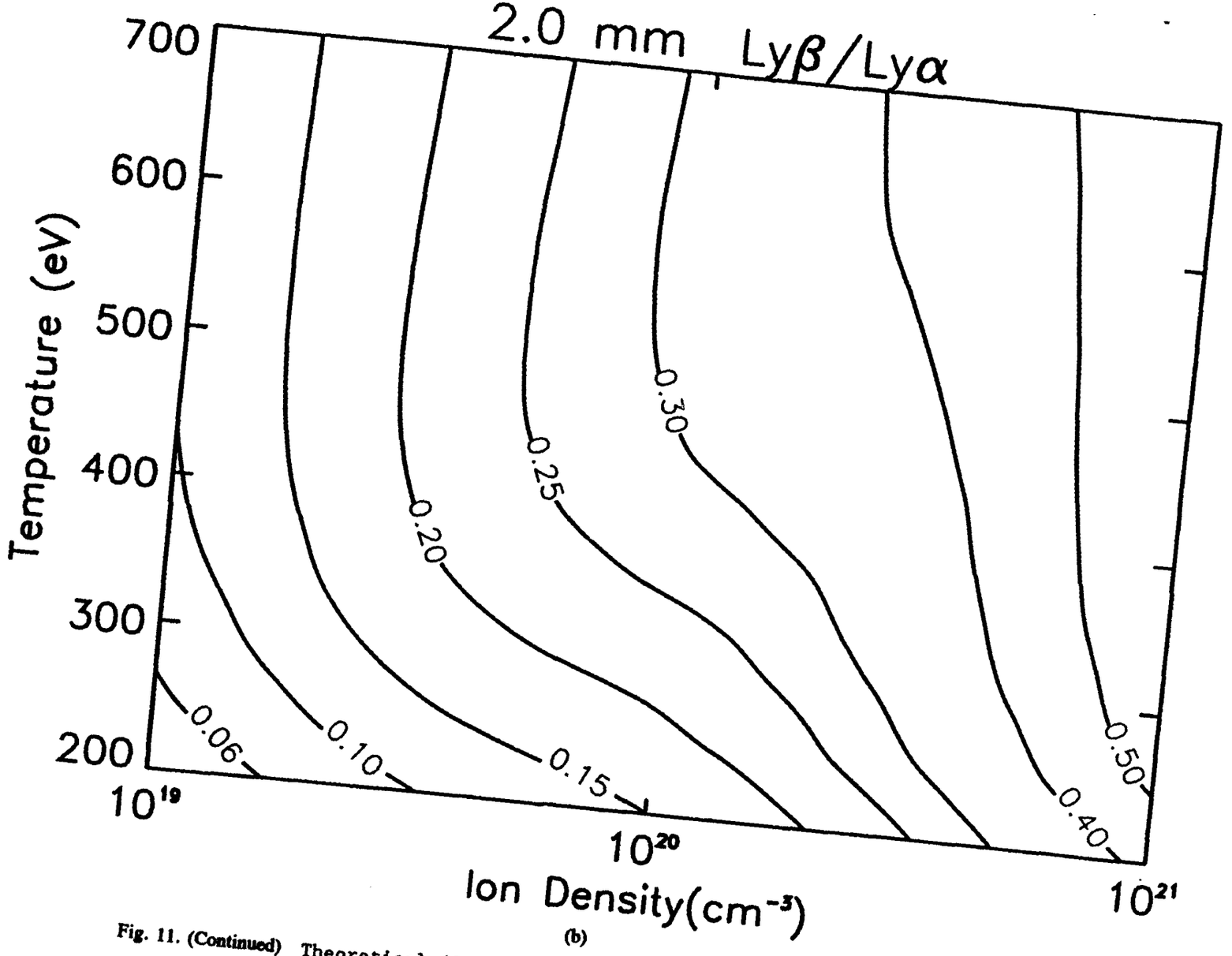

(b)

Fig. 11. (Continued) Theoretical (CRE) predicted hydrogenlike beta/alpha line ratios.

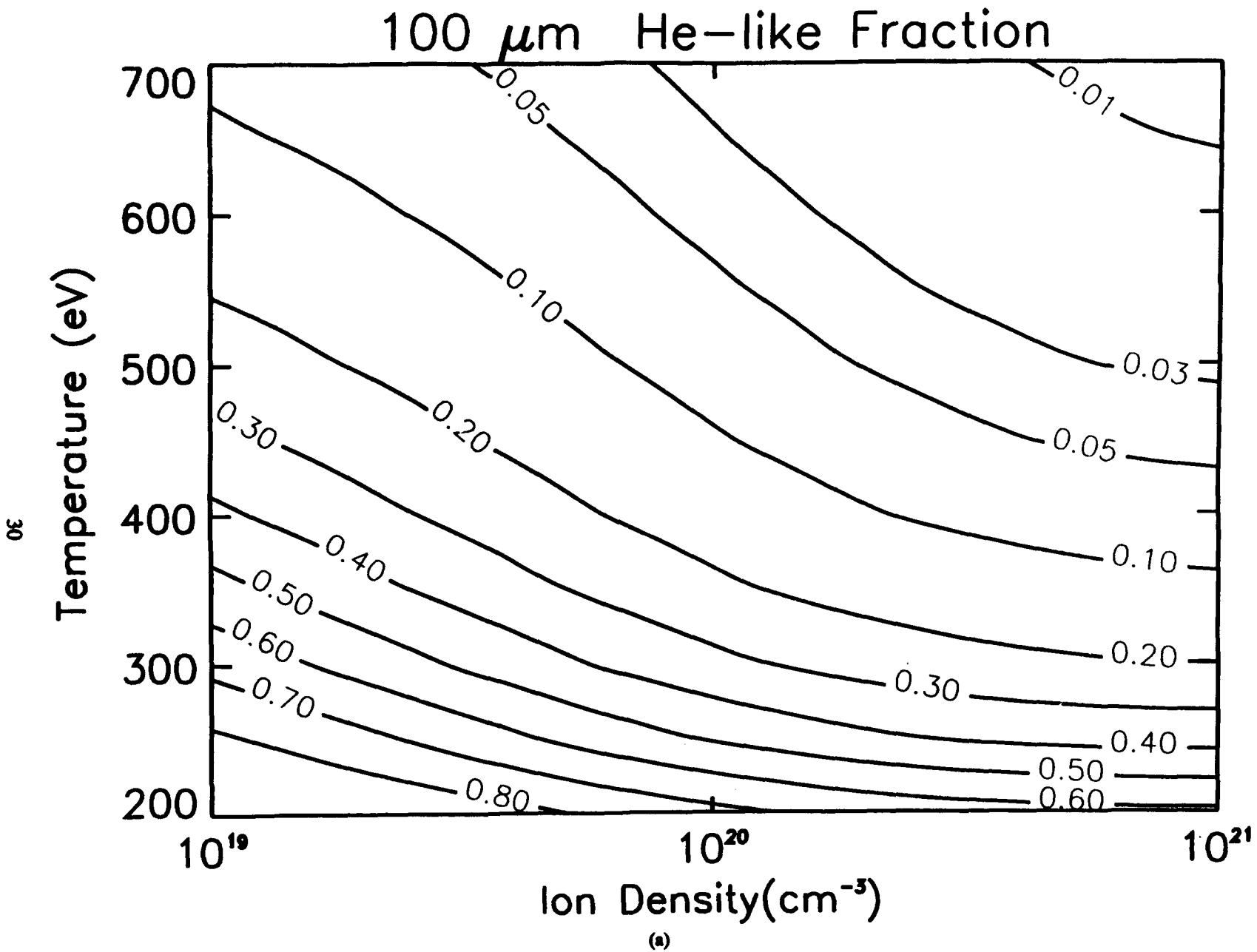

(a)

Fig. 12. Theoretical heliumlike Na abundance curves for 100 μm and 2.0 mm diameter plasmas.

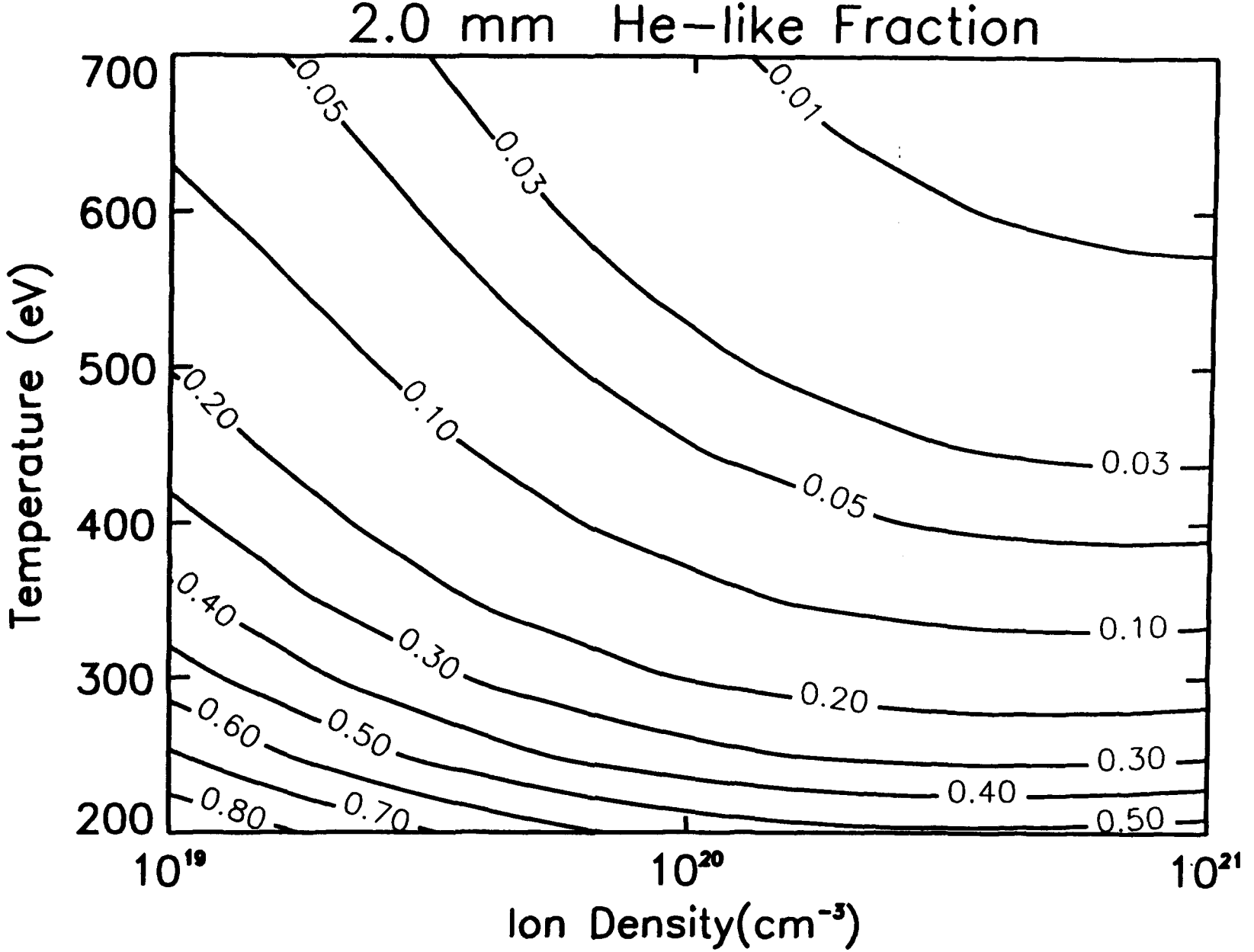

(b)

Fig. 12. (Continued) Theoretical heliumlike Na abundance curves for 100 μm and 2.0 mm diameter plasmas.

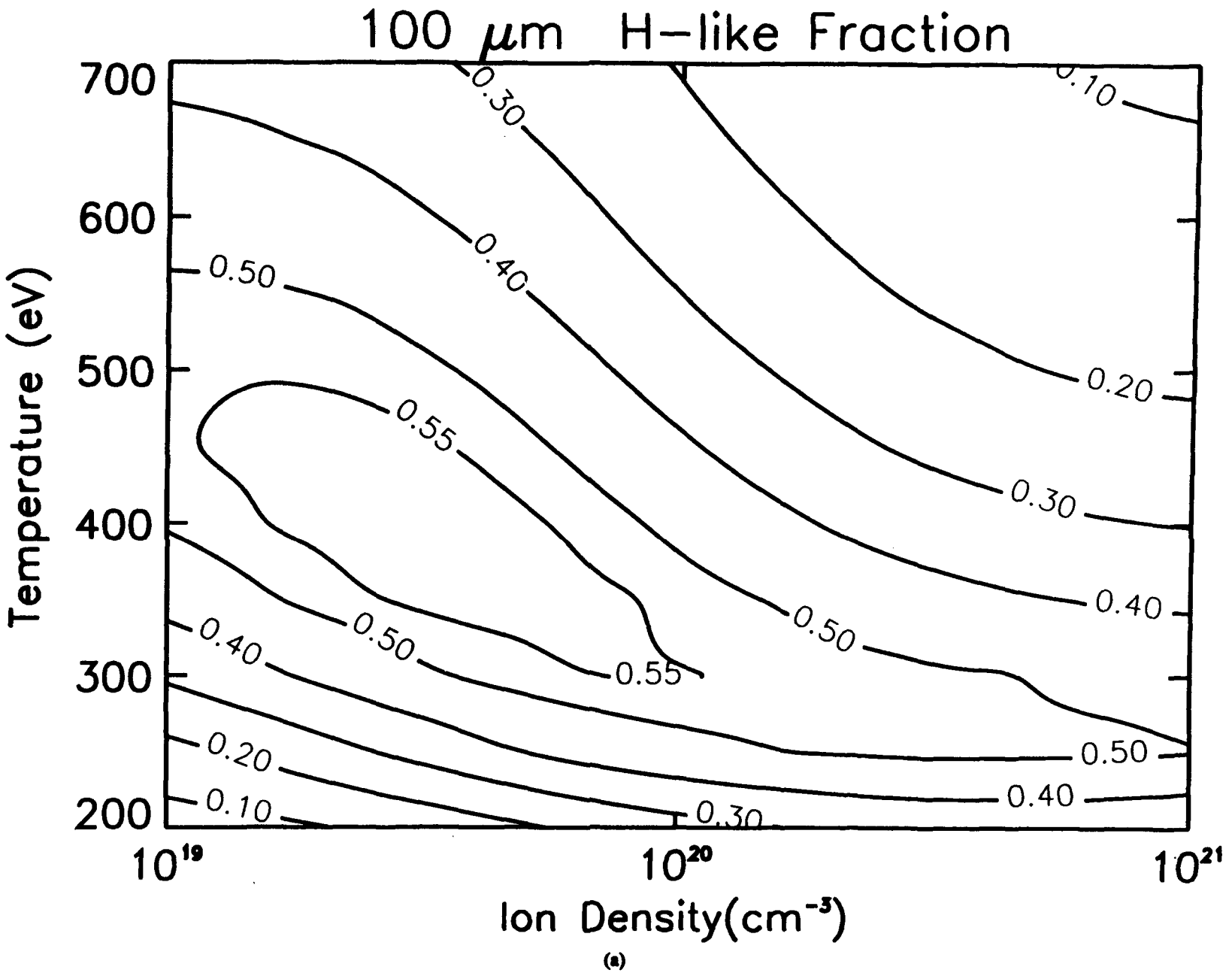

(a)

Fig. 13. Theoretical hydrogenlike Na abundance curves for 100 μm and 2.0 mm diameter plasmas.

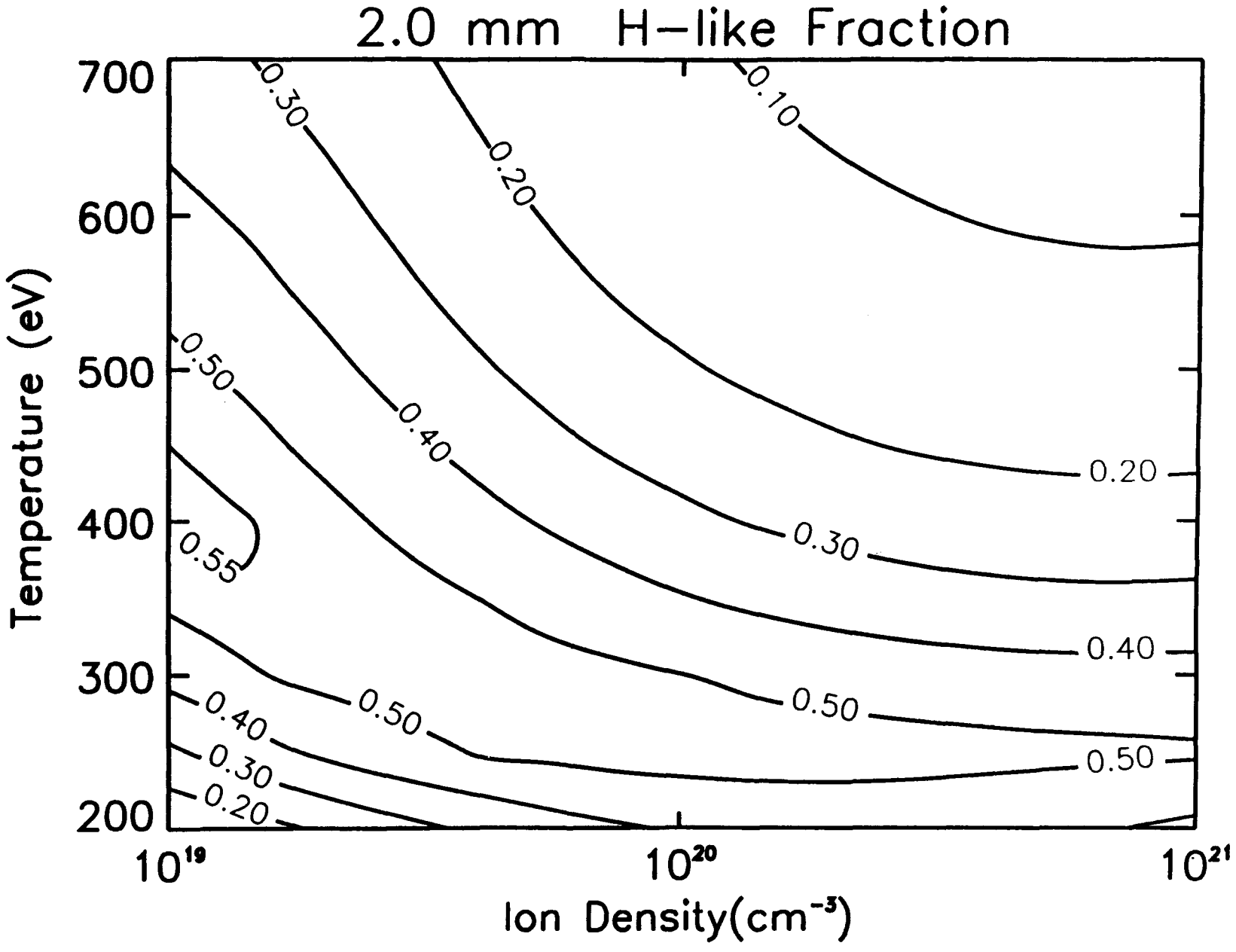

(b)

Fig. 13. (Continued) Theoretical hydrogenlike Na abundance curves for 100 μm and 2.0 mm diameter plasmas.

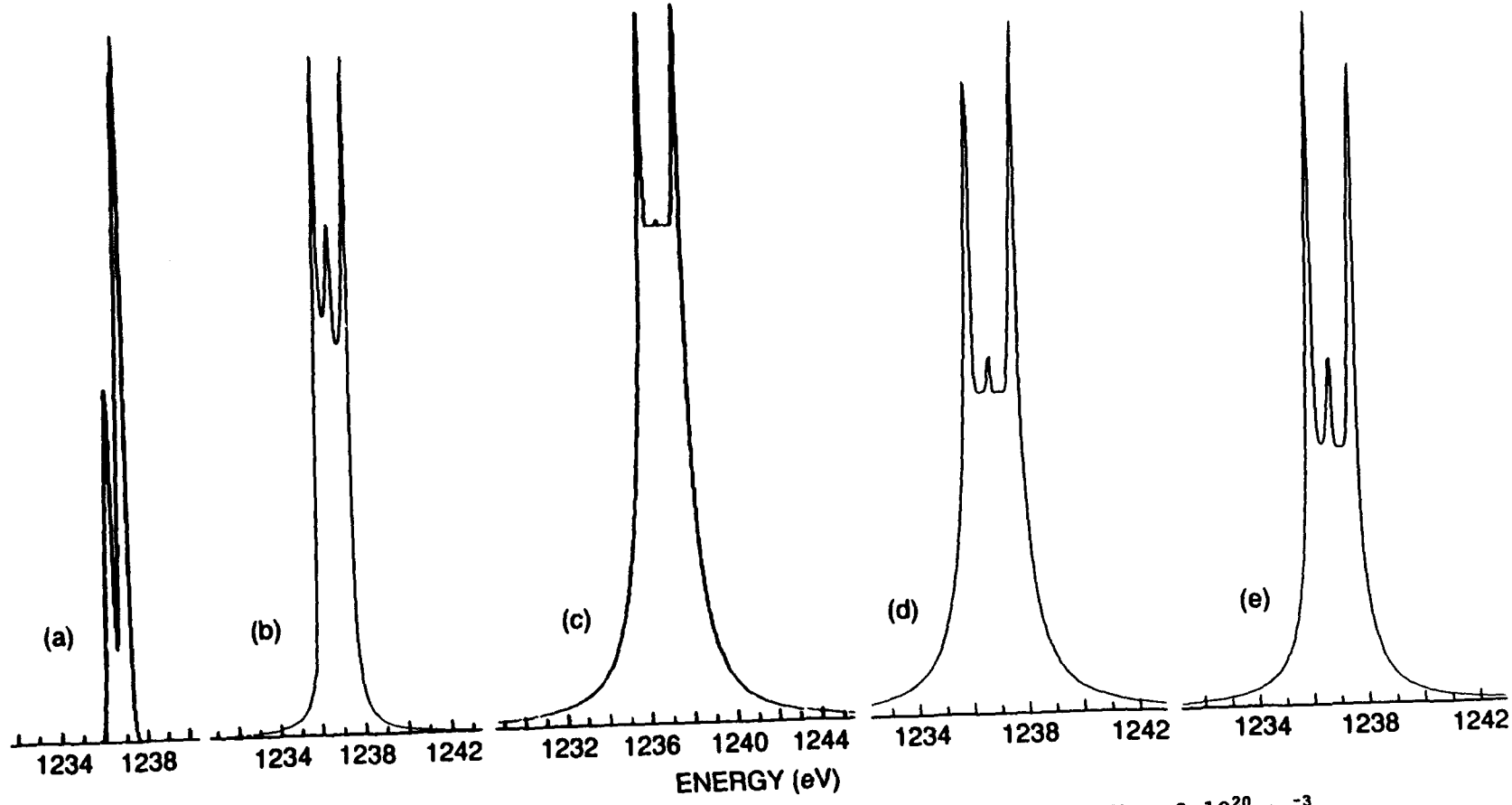

Fig. 14. Predicted sodium Ly α line profiles for plasma conditions: $N_I = 3 \cdot 10^{20}$ cm^{-3}, $T_e = 310$ eV assuming x-ray transport for plasma depths simulating a) thin, b) 110 micron, and c) 1.0 mm thicknesses and for a d) composite emission from a plasma ion density of $6 \cdot 10^{20}$ cm^{-3} for inner 100 micron region and an ion density of $1 \cdot 10^{20}$ cm^{-3} simulating a 2.0 mm diameter plasma column at plasma temperature of 300 eV and e) same as d) except reduced ion density for the plasm column: $5 \cdot 10^{19}$ cm^{-3} for 2.0 mm plasma.

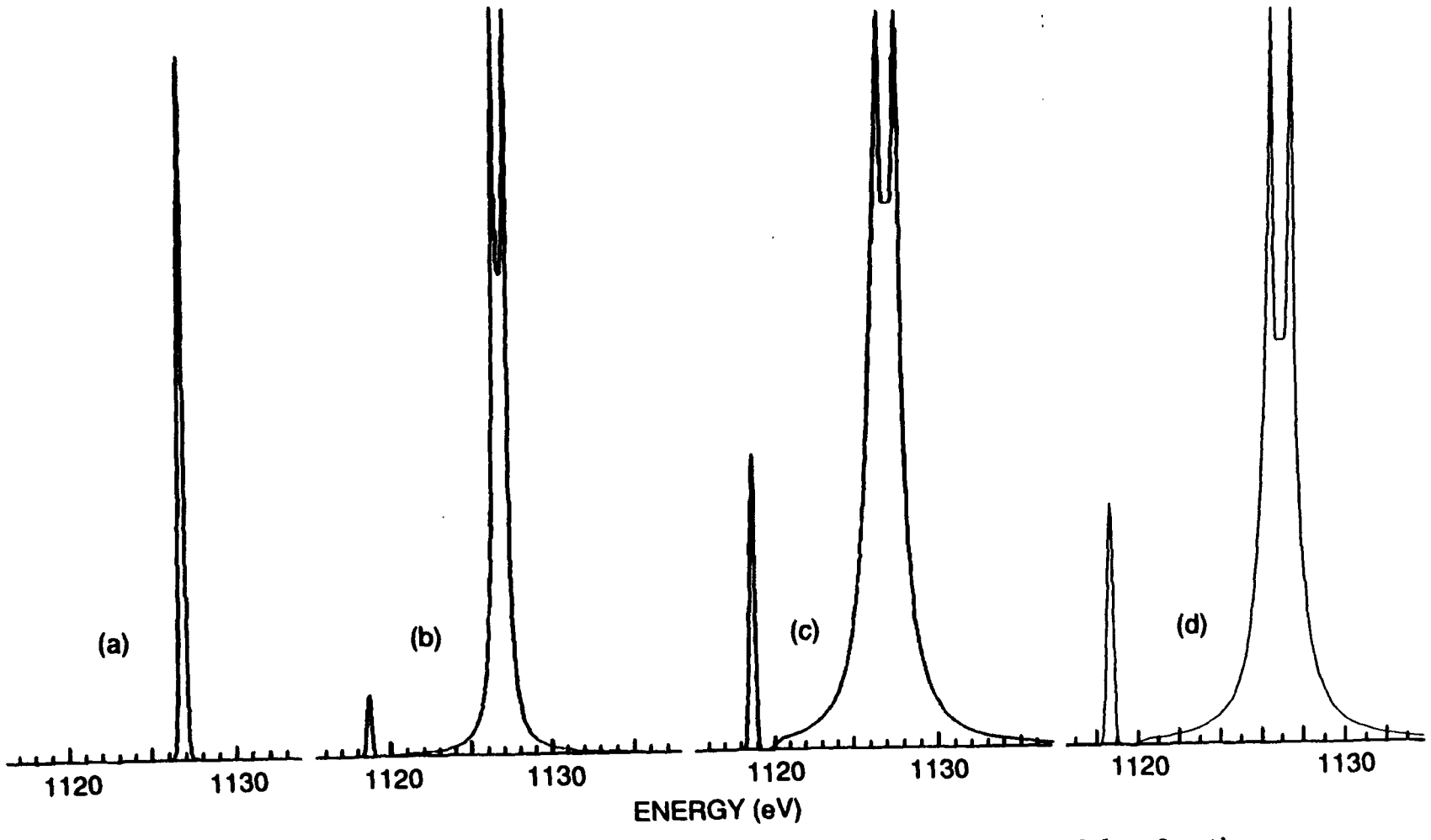

Fig. 15. Predicted sodium He α resonant and intercombination line profiles for the same plasma conditions as in Fig. 14.